PRAMANA
— journal of
physics

Vol. 43, No. 4,
October 1994
pp. 319–337

Distribution of fusion barriers

A K MOHANTY and S K KATARIA
Nuclear Physics Division, Bhabha Atomic Research Centre, Bombay 400085, India

MS received 14 February 1994; revised 16 June 1994

Abstract. Heavy ion fusion cross sections and compound nucleus average spin values obtained from distribution of fusion barriers are discussed. Various shapes of distribution functions are studied using a truncated Gaussian distribution function (TGD). It is shown that fusion cross section and average spin values are less sensitive to different parametrization of TGD function, whereas the second derivative of the product of energy and fusion cross sections (w.r.t. energy), obtained from the corresponding TGD functions are significantly different depending on the shape of the barrier distribution function. It is also shown by χ^2 analysis of fusion cross section data that some systems favour a narrow Gaussian distribution function whereas others, for which the vibrational and rotational collective states are less important, favour a flat barrier distribution. A physical interpretation of the dynamical process that gives rise to different barrier distribution is given in the framework of microscopic coupled channel calculations.

Keywords. Distribution of fusion barriers; fusion cross sections; spin distributions; simultaneous coupling; sequential coupling.

PACS Nos 25·70; 24·10

1. Introduction

Heavy ion fusion excitation functions and compound nucleus spin distributions are not yet understood fully in spite of extensive work in this field [1]. Various models have been used to understand the enhancement of fusion cross sections and broadening of spin distributions at energies near and below the Coulomb barrier. It is seen that, when energy approaches the Coulomb barrier, coupling to various low lying states [2], nucleon transfer [3,4] and neck formation [5,6] become quite important in giving rise to sub-barrier enhancement. While the above physical processes are different from each other, one common feature is that the fusing system finds a distribution of barriers. Thus one can write the fusion cross section as

$$\sigma_f(E) = \sum_l \int_0^\infty D(B)\sigma_l(E,B)\mathrm{d}B \tag{1}$$

where $\sigma_l(E,B)$ is the fusion probability for a given partial wave l and barrier height B. $D(B)$ is the probability distribution function of barrier height B where

$$\int_0^\infty D(B)\mathrm{d}B = 1. \tag{2}$$

Various shapes of barrier distribution function $D(B)$ required to fit the experimental $\sigma_f(E)$ have been explored. A well-known example is the Gaussian distribution of

barrier heights predicted for colliding nuclei undergoing slow deviations from sphericity [7]. In some cases, fits were generally obtained with flat distributions characterized by sharp cut-off values at the low energy [8,9]. This cut-off barrier height is correlated with the separation energies of the valence neutrons which has led to the conclusion that the neutron flow is the principal enhancement mechanism and that coupling to collective states plays a secondary role. This idea gets further support from the study of Rowley *et al* [10], where they derive the true barrier distribution from the second derivative of the product of energy and fusion cross section and it is shown that this quantity becomes quite broad when many neutron transfer channels are treated sequentially. Similarly, it was shown from precise experimental fusion cross section measurements [11] that the distribution function is asymmetric for deformed systems as expected on the basis of Wong's model where static deformation of both projectile and target are taken into account [12]. It is also known that in a normal coupled channel equations, where non-elastic channels are coupled directly to the elastic channel (this coupling scheme is called simultaneous coupling in ref. [10]), the resulting barrier distribution, having two significant peaks, is quite different. With increasing number of channels, these two peaks separate further. Therefore, one hopes to learn more about the mechanism of channel coupling from the underlying barrier distribution function which is different for different coupling mechanisms and this difference is not too obvious from the analysis of the fusion excitation function or from the average spin values.

In this work, we have studied in depth several barrier distribution functions which fit the experimental data. Different shapes of barrier distribution functions are generated by using a truncated Gaussian distribution function (TGD) where the width δ and the truncation limit t are taken as parameters. In § 1, experimental fusion cross sections are fitted for several systems using TGD function with different width parameter δ and t is adjusted for each δ in order to achieve the best fit. Various shapes of barrier distribution function starting from flat shape to narrow Gaussian shape can be used and all of them fit fusion cross sections and average spin values quite well. In other words, fusion cross sections and average spin values are less sensitive to different parametrizations of barrier distribution function. It is shown in § 2 that the effect of different parametrization can be seen prominently in the quantity $d^2(\sigma_f E)/dE^2$ which is quite different for different barrier distribution functions and therefore, carry more discriminating features. The available experimental fusion data for a large number of H. I. systems have been analysed using TGD parametrization and a careful χ^2 analysis of experimental fusion data shows that some systems favour a Gaussian barrier distribution while others favour a flat barrier distribution i.e. a TGD function with large width. In the last section, we give a qualitative interpretation to these observations in the framework of microscopic coupled channel calculations.

2. Fusion cross section and spin distribution

Heavy ion fusion cross section at a given energy E and partial wave l for a given barrier height B can be written as

$$\sigma_l(E, B) = (\pi/k^2)(2l + 1)\, T_l(E, B) \tag{3}$$

where $T_l(E, B)$ is the corresponding tunneling probability and can be calculated using

a simple barrier penetration model as given by

$$T_l(E,B) = \{1 + \exp[(2\pi/\hbar\omega)(B - E - l(l+1)\hbar^2/2\mu R_0^2)]\}^{-1} \tag{4}$$

where μ is the reduced mass in the entrance channel and R_0 is the fusion barrier radius. Therefore, $\sigma_l(E)$ summed over all barriers can be obtained from eq. (1), where $D(B)$ is chosen to have a Gaussian shape and is given by

$$D(B) = N\exp[-(B - V_0)^2/2\delta^2] \tag{5}$$

where N is the normalization constant and V_0 the average barrier height that explains the high energy fusion cross section. Similarly, average spin can be written as

$$\langle l \rangle = \frac{\Sigma l\sigma_l(E)}{\Sigma\sigma_l(E)}. \tag{6}$$

In the present analysis, it is difficult to fit fusion cross section for many systems using only a Gaussian distribution function. However, most of these experimental data can be fitted using TGD parametrization. This method has been used earlier by Reisdorf *et al* [13] to fit experimental cross sections for Ar^+ (Sm, Sn) systems. They find that the data are reproduced well when the Gaussian distribution is truncated at a limit δt, where δ is related to the deformation length β and t value lies between 2 and 3. Therefore, with TGD parametrization, eq. (1) is integrated from $V_0 - \delta t$ to $V_0 + \delta t$ instead of 0 to ∞. The normalization constant N is obtained from the relation

$$N\int_{V_0-\delta t}^{V_0+\delta t} D(B)\mathrm{d}B = 1. \tag{7}$$

In the least square analysis of fusion excitation functions, both parameters δ and t are varied so as to obtain minimum chi-square (χ^2) per degrees of freedom. Figure 1(a), shows the fitted fusion excitation function for three systems e.g. $^{40}Ar + {}^{122}Sn$, $^{58}Ni + {}^{64}Ni$ and $^{16}O + {}^{154}Sm$ with TGD parametrization for three different values of δ and figure 1(b), shows the corresponding derived average spin values. The truncation limit t for each system was obtained by minimizing χ^2 for a given value of width parameter δ. It can be seen from figure 1(a) that all the three fits are indistinguishable from each other and reproduce the experimental fusion cross sections rather well. The derived average spin values (see figure 1(b)) obtained from different width parameter δ are also indistinguishable from each other and this holds true for all other systems studied. The minimum values of χ^2/N as a function of δ are shown in figure 2 for various systems. These values along with various potential parameters used in the fits are listed in table for all the systems. As seen from figure 2, χ^2/N is very shallow as a function of δ for many systems, whereas for systems like Ar + Sm and Ge + Ge, where the t values are quite large, well defined minima are obtained. In these cases, χ^2/N changes significantly with any small change in δ parameter. For remaining systems, χ^2/N values for a sharp Gaussian distribution ($\delta = 4$ MeV) and for a flat distribution ($\delta = 20$ MeV) do not differ much and for these systems t values are rather small. In other words, a range of TGD functions for $D(B)$ can be used to fit the same experimental fusion data with similar quality of fits. On the other hand, if we look at the corresponding barrier dsitribution, (see figure 1(c)

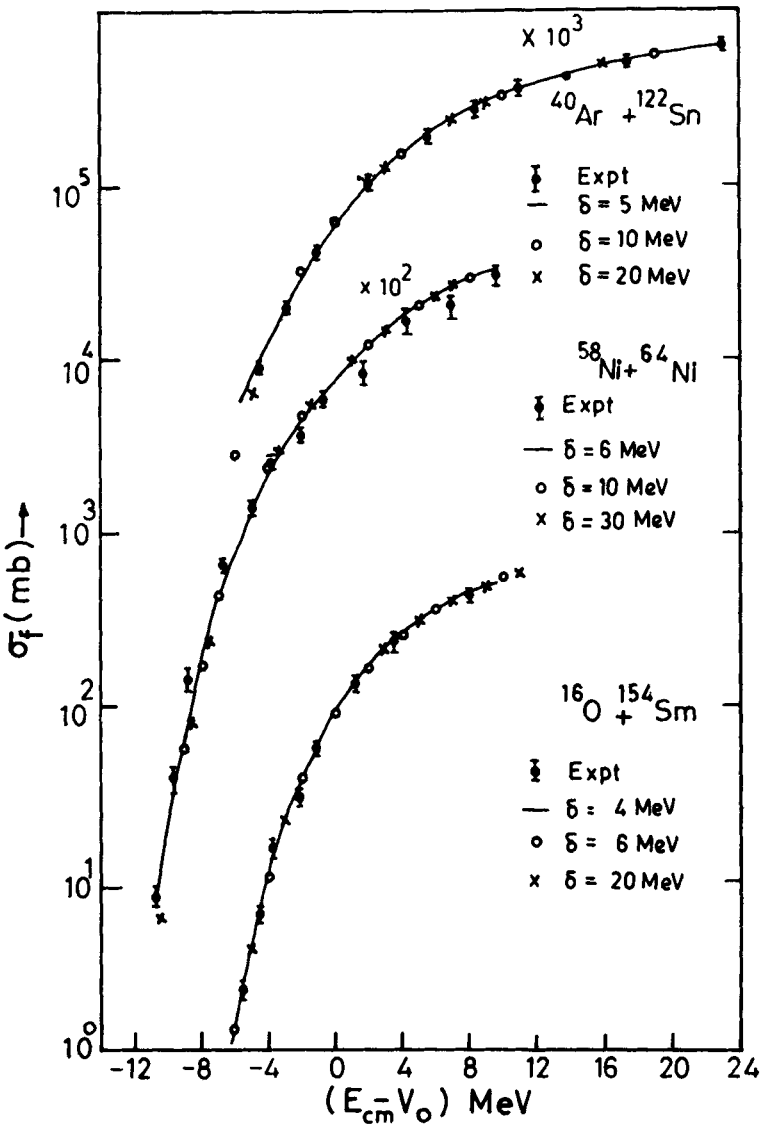

Figure 1(a). Fusion cross section versus $(E_{cm} - V_0)$ for $^{40}Ar + ^{122}Sn$, $^{58}Ni + ^{64}Ni$ and $^{16}O + ^{154}Sm$ systems for three different δ values shown in figure. The δ and t values are (5, 1·55), (10, 0·688), (20, 0·336) for $^{40}Ar + ^{122}Sn$ system, (6, 1·52), (10, 0·86) and (30, 0·275) for $^{58}Ni + ^{64}Ni$ system, (4, 1·47), (6, 0·92) and (20, 0·265) for $^{16}O + ^{154}Sm$ system. Experimental points are taken from refs. [13, 23, 21].

for $^{16}O + ^{154}Sm$ and $^{58}Ni + ^{64}Ni$ systems) they are completely different. There is a lower limit to δ, beyond which the distribution becomes narrow and it is not possible to reproduce fusion cross section.

Using one dimensional barrier penetration model for fusion to calculate fusion probability $\sigma_l(E, B)$ for a given barrier height B (Using (3) and (4)) and replacing the summation over l by an integral, eq. (1) can be written as

$$\sigma_f(E) = \int D(B)\sigma_w(E, B)\mathrm{d}B \tag{8}$$

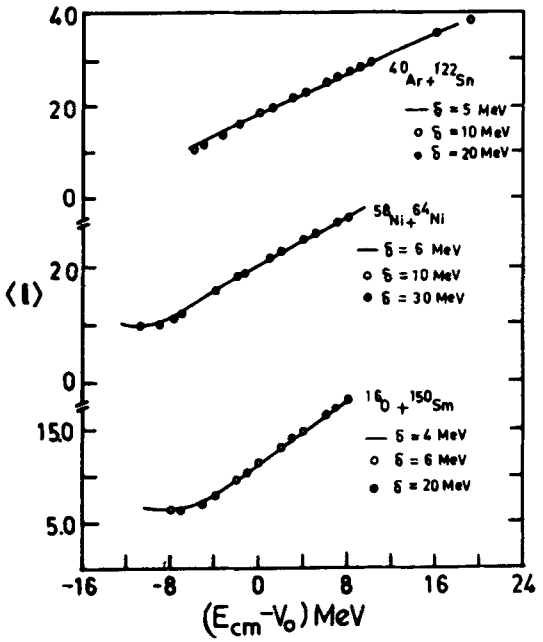

Figure 1(b). Average compound nucleus spin values versus $(E_{cm} - V_0)$ for $^{40}Ar + ^{122}Sn$, $^{58}Ni + ^{64}Ni$ and $^{16}O + ^{154}Sm$ for δ values used to fit fusion cross-section in figure 1(a).

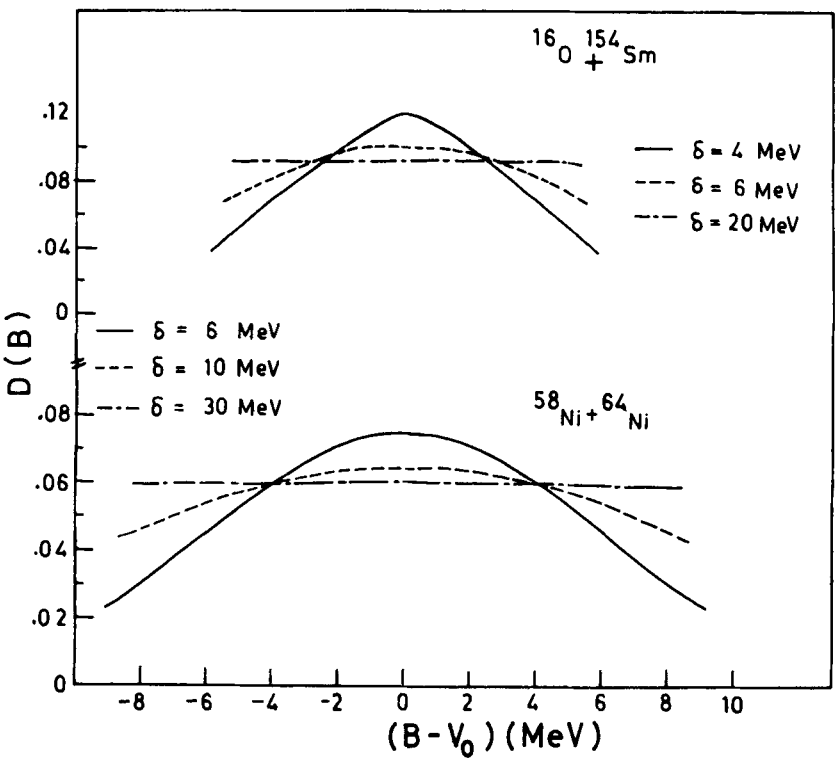

Figure 1(c). Barrier distribution function versus $(E_{cm} - V_0)$ for $^{16}O + ^{154}Sm$ and $^{58}Ni + ^{64}Ni$ systems for δ values used to fit fusion cross-section in figure 1(a).

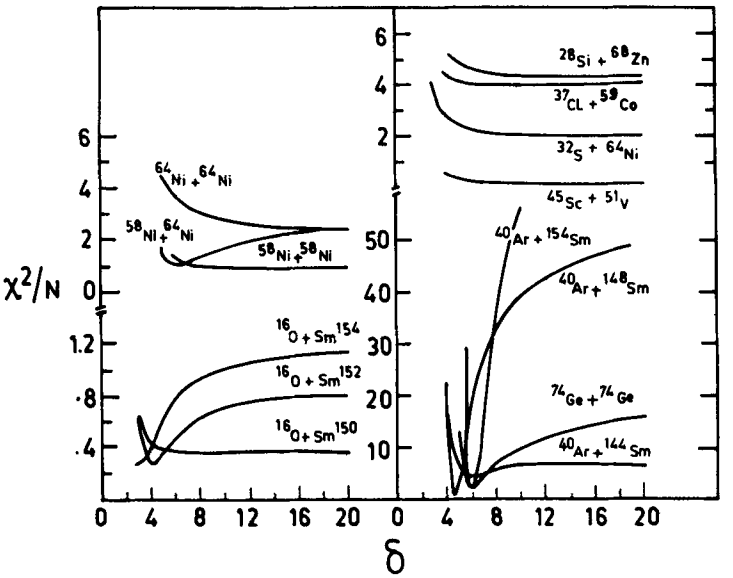

Figure 2. Minimum χ^2/N versus δ for different systems. For each δ, the value of t is adjusted to obtain minimum χ^2/N.

where $\sigma_w(E, B)$ is the l integrated fusion cross-section for a given barrier height B given by Wong's formula [12]

$$\sigma_w(E, B) = (\hbar\omega R_0^2/2E)\log\{1 + \exp[2\pi/\hbar\omega(E - B)]\} \tag{9}$$

In the above, the integration variable B varies from $V_0 - \delta t$ to $V_0 + \delta t$. For very large width, δt approaches a constant value and $D(B)$ can be approximately expressed as an uniform distribution given by $(2\delta t)^{-1}$. The fusion cross section for this uniform distribution can be written from eq. (8) as

$$\sigma_f = (2\delta t)^{-1} \int_{V_0 - \delta t}^{V_0 + \delta t} \sigma_w(E, B)\mathrm{d}B.$$

For $E \gg B$, the above integral reduces to

$$\sigma_f(E) = (2\delta t)^{-1} \int_{V_0 - \delta t}^{V_0 + \delta t} (\pi R_0^2/E)(E - B)\mathrm{d}B \tag{10}$$

which is very much similar to Stelson's barrier expression [8] except for the upper limit of integration. In Stelson's notation, $V_0 - \delta t$ represents the threshold barrier B_t for neutron flow and $D(B)$ is $[2(V_0 - B_t)]^{-1}$ in the range B_t and $(2V_0 - B_t)$ and zero outside this range. Stelson further sets $D(B)$ to zero for $E \leqslant 2V_0 - B_t$. Therefore, replacing the upper limit of integration in eq. (8) by E, one gets Stelson's expression

$$\sigma_f(E) = (\pi R_0^2/4)(V_0 - B_t)^{-1}(E - B_t)^2/E \tag{11}$$

for $E \leqslant 2V_0 - B_t$. This threshold barrier B_t is correlated by the above author with the separation energies of the valence neutrons and is related to the distance at which projectile and target potentials just allow neutrons to flow between the nuclei. As an

Table 1. The width δ of the distribution function and the corresponding truncation limit t are listed for many systems for which χ^2/N is minimum. The potential parameters $\hbar\omega$, R_0 and V_0 are taken from the systematics that explains the fusion cross-section at high energies. N is the number of data points.

System	δ	t	δt	χ^2/N	$\hbar\omega$	R_0	V_0	N	Ref.
$^{16}O + ^{154}Sm$	3·0	2·24	6·72	0·279	4·5	11·2	60	8	[21]
$^{16}O + ^{152}Sm$	4·0	1·32	5·28	0·26	4·5	11·2	60	7	[21, 22]
$^{16}O + ^{150}Sm$	8·0	0·537	4·29	0·363	4·5	11·2	60	8	[21]
$^{40}Ar + ^{154}Sm$	6·0	2·83	16·98	2·20	4·5	11·2	127·4	14	[13]
$^{40}Ar + ^{148}Sm$	4·5	2·89	13·01	1·07	4·5	11·2	128·4	12	[13]
$^{40}Ar + ^{144}Sm$	6·0	1·39	8·34	4·81	4·5	11·2	128·6	11	[13]
$^{40}Ar + ^{122}Sn$	20·0	0·336	6·72	1·93	4·5	11·2	106	12	[13]
$^{58}Ni + ^{64}Ni$	6·0	1·52	9·12	1·05	4·5	11·2	100	27	[23]
$^{64}Ni + ^{64}Ni$	20·0	0·372	7·44	2·40	4·5	11·2	97·8	13	[23]
$^{58}Ni + ^{58}Ni$	20·0	0·38	7·60	0·940	4·5	11·2	102	14	[23]
$^{32}S + ^{64}Ni$	20·0	0·255	5·10	2·112	4·0	10·2	59·1	14	[24]
$^{28}Si + ^{68}Zn$	20·0	0·254	5·08	8·61	4·0	9·5	56·2	14	[24]
$^{37}Cl + ^{59}Co$	10·0	0·38	3·80	8·22	4·0	9·5	56·2	14	[24]
$^{45}Sc + ^{51}V$	20·0	0·28	5·60	0·278	4·0	10·7	64	8	[24]
$^{74}Ge + ^{74}Ge$	6·0	2·9	17·4	3·14	4·2	10·5	125·4	25	[25]

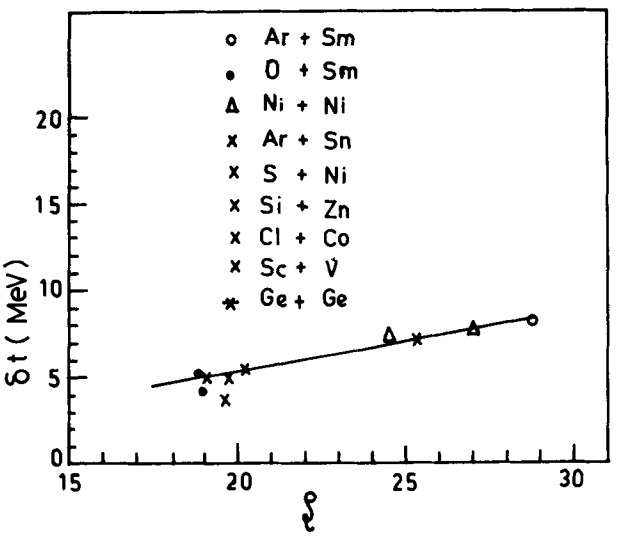

Figure 3. The optimal δt value versus effective fissility ξ for the systems which favour flat barrier distribution function.

example, based on some model calculation for $^{58}Ni + ^{58}Ni$ and $^{64}Ni + ^{64}Ni$ systems he finds B_t values around 94·2 and 89·2 MeV, the corresponding values of the lower limit of barrier distribution ($V_0 - \delta t$) as obtained in present analysis are 94·4 and 90·36 MeV (see table for above two systems at $\delta = 20$ MeV) which are in good agreement.

Similarly for $^{58}Ni + ^{64}Ni$ system, although a flat barrier distribution gives an accepetable fit, χ^2/N minimization occurs at $\delta = 6$ MeV which corresponds to a Gaussian barrier distribution. This suggests that the mechanism which gives results

in barrier distribution in $^{58}Ni + ^{64}Ni$ system is quite different from that of $^{58}Ni + ^{58}Ni$ and $^{64}Ni + ^{64}Ni$ systems. Except for $O + ^{152,154}Sm$, $Ar + Sm$, $Ge + Ge$ and $^{58}Ni + ^{64}Ni$ systems, the remaining system favours a flat distribution function. Figure 3 shows the plot of optimal δt (δt for which χ^2/N is minimum) versus ξ for all the systems which favour a flat barrier distribution listed in table where the effective fissility ξ is defined as

$$\frac{4Z_1Z_2}{A_1^{1/3}A_2^{1/3}(A_1^{1/3}+A_2^{1/3})}.$$

It is seen that the optimal δt values increase monotonically with ξ. As pointed out by Aguair *et al* [14] and Krappe *et al* [15], this dependence of the width δt on fissility parameter ξ can be correlated to the concept of neck formation or neutron flow which depends on the liquid drop model properties of the colliding partners.

3. Determination of distribution of barriers from fusion cross section

The differences in fusion cross sections can be seen prominently in the quantity $d^2(\sigma_f E)/dE^2$ as calculated for different barrier distribution functions [10, 16]. From (8) and (9), one can write

$$(\sigma_f E) = \pi R_0^2 \int D(B)\, L(x) dB, \tag{12}$$

$$\frac{d}{dE}(\sigma_f E) = \pi R_0^2 \int D(B)\, T(x) dB, \tag{13}$$

$$\frac{d^2}{dE^2}(\sigma_f E) = \pi R_0^2 \int D(B) G(x) dB. \tag{14}$$

The limits of integration on the right hand side are from $V_0 - \delta t$ to $V_0 + \delta t$

$$x = (2\pi/\hbar\omega)(E - B),$$

$$L(x) = (\hbar\omega/2\pi)\log[1 + \exp(x)],$$

$$T(x) = dL(x)/dx = [1 + \exp(-x)]^{-1},$$

$$G(x) = dT(x)/dx = (2\pi/\hbar\omega)\exp(x)/[1 + \exp(x)]^2.$$

As seen above, the integral in (12) is related to fusion cross section. The first derivative in (13) relates to the s-wave transmission T_0 at energy E. Similarly, the second derivative in (14) gives a direct measure of the barrier distribution function $D(B)$. The function $G(x)$ is a narrow width symmetric function and becomes a delta function in the limit $\hbar\omega \to 0$. Therefore, (14) can be written as

$$\frac{d^2}{dE^2}(\sigma_f E) = \pi R_0^2 \bar{D}(E) \tag{15}$$

where $\bar{D}(E)$ is the underlying barrier distribution smoothed by the function $G(x)$. Therefore, it is possible to extract a meaningful barrier distribution function from the above second derivative. It can also be seen that (13) gives the slope of the function

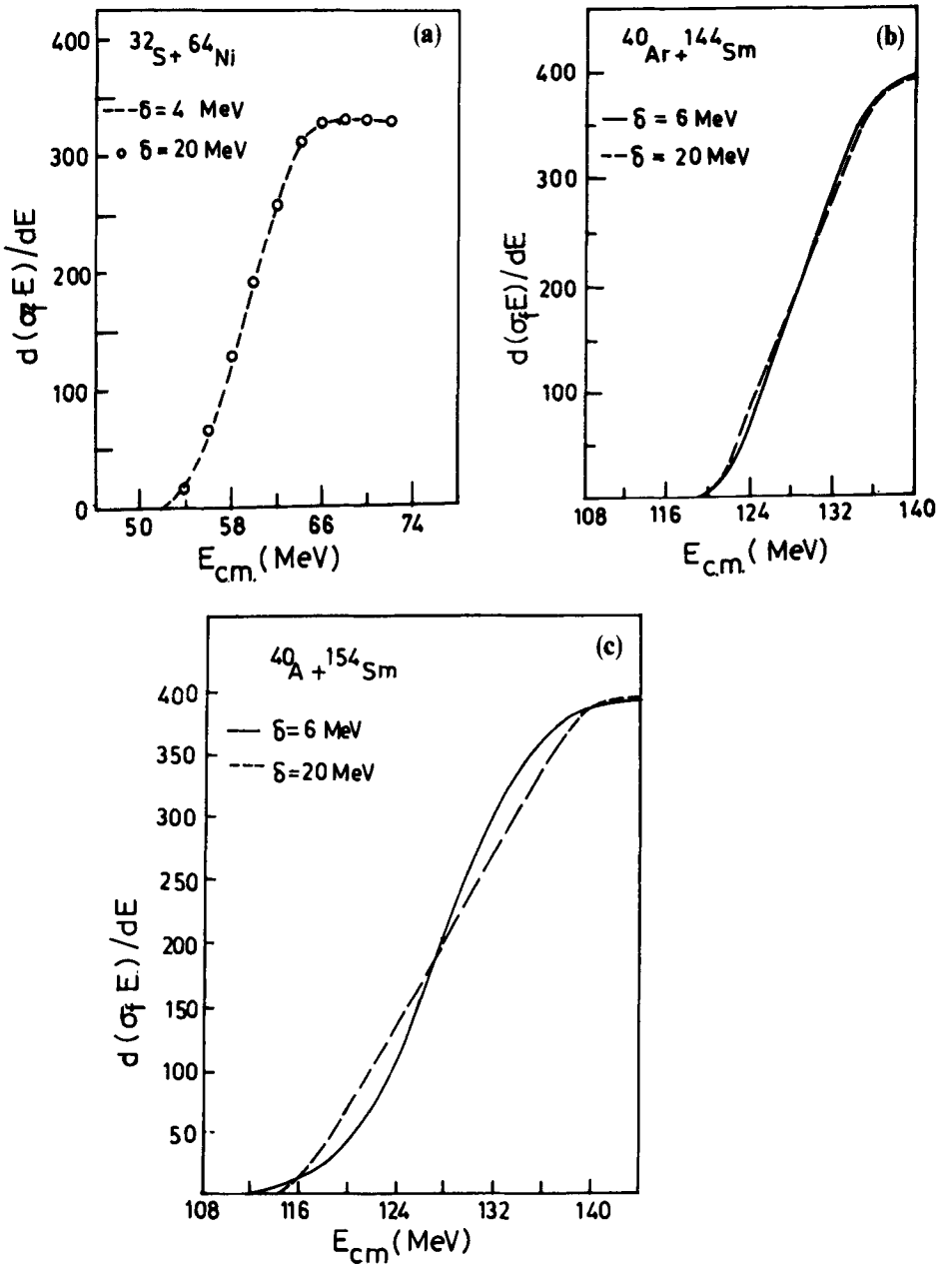

Figure 4(a, b, c). $d(\sigma_f E)/dE$ versus $E_{c.m.}$ for three typical systems with two different widths δ.

$(\sigma_f E)$. Therefore, any difference in the calculated fusion cross sections will get reflected through its first derivative which is the transmission coefficient T_0 at energy E. Similarly any differences in transmission coefficient can be seen prominently by its derivative as given by (14). Figures 4 and 5 show the plot of $d(\sigma_f E)/dE$ and $d^2(\sigma_f E)/dE^2$ as a function of energy E for three typical systems ($^{32}S + ^{64}Ni$ and $^{40}Ar + ^{144}Sm$ and $^{40}Ar + ^{154}Sm$) at two values of δ. The differences in first derivatives obtained from two extreme shapes of barrier distribution function are not significant for $^{32}S + ^{64}Ni$

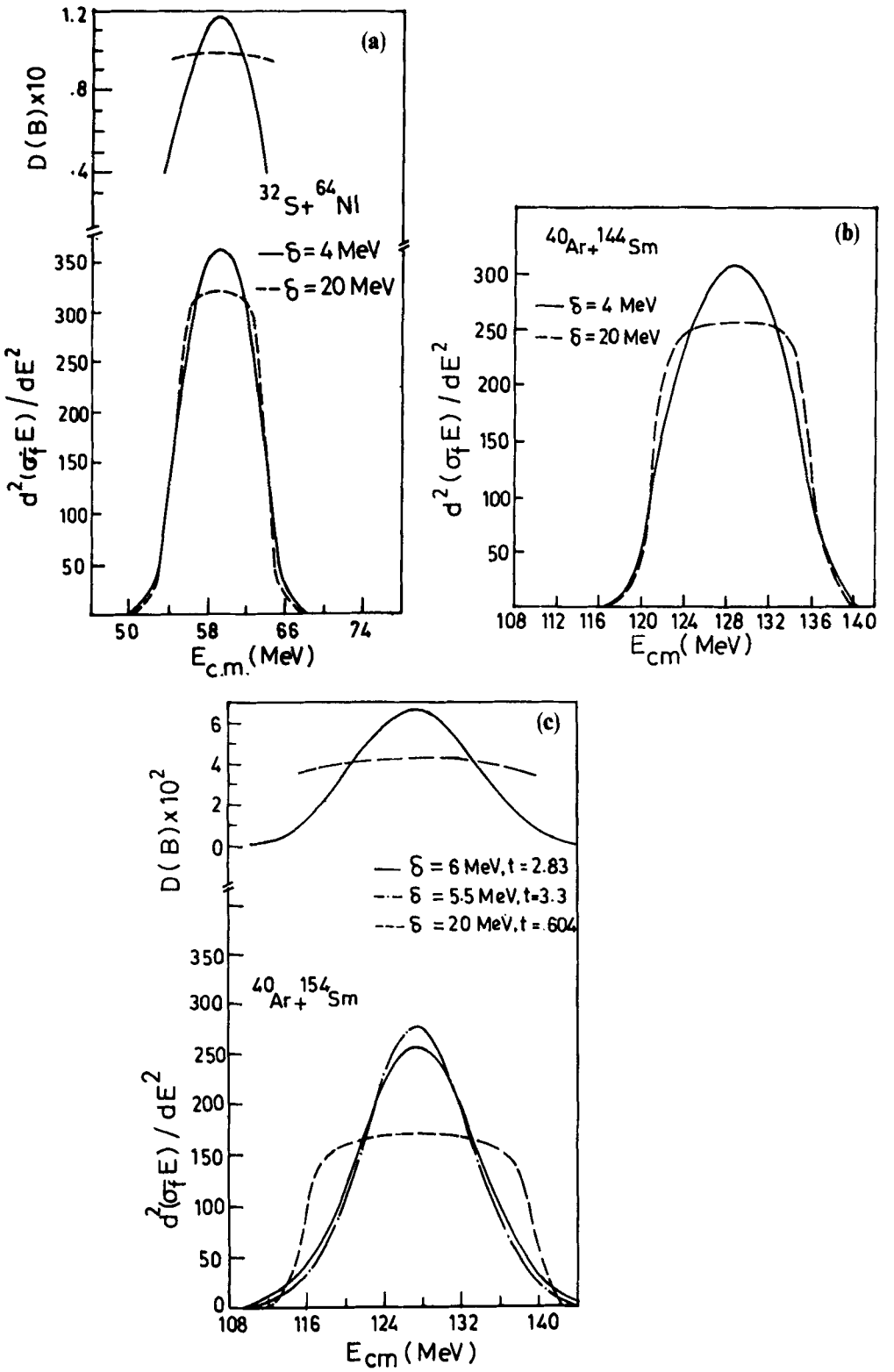

Figure 5(a, b, c). $d^2E(\sigma_f E)/dE^2$ versus $E_{c.m.}$ for the same system as that of figure 4. The upper part in figures 5(a) and 5(c) show the corresponding barrier distribution function.

and $^{40}Ar + ^{144}Sm$ systems (see figure 4). For $^{32}S + ^{64}Ni$ system, χ^2/N is minimum for $\delta = 20$ MeV ($t = 0{\cdot}255$) and for $^{40}Ar + ^{144}Sm$, χ^2/N is minimum for $\delta = 6$ MeV ($t = 1{\cdot}39$). For other values of δ, χ^2/N increases. However, this increase is not strong enough to bring out any significant differences in fusion cross section or in the average spin values. On the other hand, these small differences have become more distinct in figure 5 which relates to the true barrier function $D(B)$ smoothed by the function $G(x)$. Therefore, it is possible to extract the shape of the barrier distribution function from the experimental fusion cross-section as has been done for $^{16}O + ^{154}Sm$ system [11]. Even though, the second derivative is different for different $D(B)$ function, it is interesting to note that, in $^{32}S + ^{64}Ni$ (see figure 5(a)), this difference is seen only around the maximum whereas the width does not differ much. For such systems, which have small t values, the measurements of fusion cross-section need to be done very accurately in order to bring out this difference in distribution function. On the other hand, the system like $^{40}Ar + ^{154}Sm$, for which t is quite large, all shapes of barrier distribution function will not fit the fusion cross section as χ^2/N is minimum for a particular choice of δ and t parameters. The fits become quite poor for small changes in δ and t parameters (see figure 2). Therefore, for this type of system where the optimal δt is quite large, the barrier distribution function can be determined with greater accuracy by fitting the fusion cross-section itself. The second derivative and the distribution function $D(B)$ obtained for $\delta = 20$ MeV and $\delta = 5{\cdot}5$ MeV are also quite different as seen in figure 5(c) for the same system. In $^{16}O + ^{154}Sm$ system, as shown by Wei *et al* [11] and in the present case too, the data can be reproduced well if the distribution function is chosen to have a asymmetric Gaussian shape as shown in figure 6. In this case, the distribution function obtained from experimental

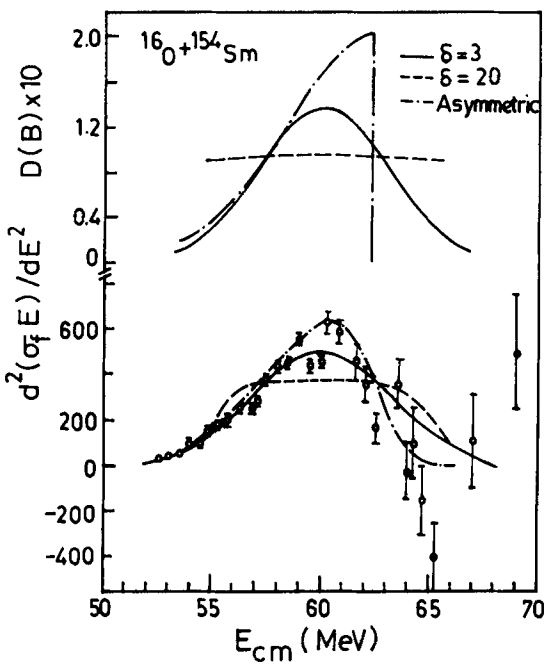

Figure 6. Same as figure 5, but for $^{16}O + ^{154}Sm$ system with $\delta = 3$ and 20 MeV and also with an asymmetric barrier shape as shown in upper part of the figure. The experimental points are taken from ref. [11].

data is asymmetric due to static deformation of ^{154}Sm and can be distinguished from a flat distribution. Even though the true barrier distribution for deformed target is asymmetric, we have considered only the symmetric distributions for simplicity.

4. Interpretation of distribution of barriers

It can be seen from figure 2 that most of the systems favour a large δ value. For these systems, the distribution function $D(B)$ is quite broad which is quite similar to that of a flat distribution. Stelson [8] often found necessary to describe heavy ion fusion cross-sections. Figure 2 shows that a few systems favour a Gaussian distribution function. In the following, we wish to understand these results in the microscopic framework of coupled channel calculations. In this approach, the set of coupled equations is solved approximately by diagonalizing the coupling matrix around the unperturbed barrier [17], which enables one to decouple the equations into a family of eigen channels where the total transmission is weighted sum of the transmission through each eigen channel given by

$$T(E) = \sum_{\alpha} |U_{\alpha 0}|^2 T_{\alpha 0}[E, V(r) + \lambda_{\alpha}(r)]. \tag{15}$$

$U_{\alpha 0}$ is the overlap probability which is evaluated at the unperturbed barrier position, $\lambda_{\alpha}(r)$ is the eigen value of the coupling matrix $M_{\alpha\beta}$. Following Rowley *et al* [10], the coupling scheme for the simultaneous and sequential inelastic and transfer as given by figures 7(a) and 7(b) is used in the following calculations. In figure 7(a), all the non-elastic channels (both inelastic and transfer) are coupled to the ground state

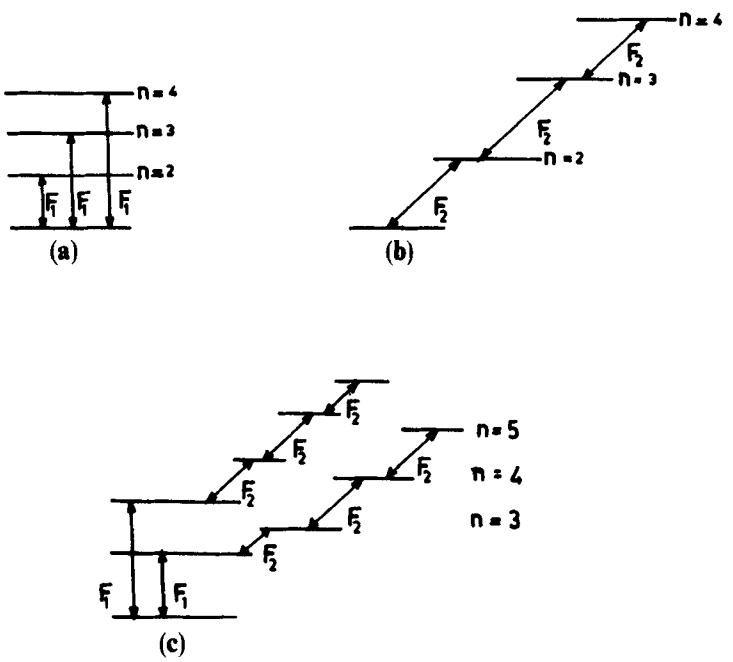

Figure 7(a). Schematic representation for simultaneous coupling; **7(b).** Schematic representation for sequential transfer; **7(c).** Schematic representation of sequential transfers that follows from the states inelastically excited.

directly and the coupling matrix is given by (as an example for $n = 5$)

$$M_{\alpha\beta} = \begin{vmatrix} 0 & F_1 & F_1 & F_1 & F_1 \\ F_1 & -Q & 0 & 0 & 0 \\ F_1 & 0 & -Q & 0 & 0 \\ F_1 & 0 & 0 & -Q & 0 \\ F_1 & 0 & 0 & 0 & -Q \end{vmatrix} \tag{16}$$

Figure 7(b) represents multinucleon transfer coupling scheme where a single nucleon (mostly neutron) transfer channel is coupled to the elastic ground state, the two neutron channel is coupled to the single neutron transfer channel, but not directly to the elastic channel. Similarly, a three neutron transfer channel is coupled to the two neutron transfer channel and so on. Accordingly, the coupling matrix is given by

$$M_{\alpha\beta} = \begin{vmatrix} 0 & F_2 & 0 & 0 & 0 \\ F_2 & -Q & F_2 & 0 & 0 \\ 0 & F_2 & -Q & F_2 & 0 \\ 0 & 0 & F_2 & -Q & F_2 \\ 0 & 0 & 0 & F_2 & -Q \end{vmatrix} \tag{17}$$

For simplicity, the coupling form factor is taken to be same at each step. In the case of neutron transfer, F_2 is taken as that of a one-particle transfer form factor given by [17]

$$F_2 = \frac{1}{(4\pi)^{1/2}}(3\,\text{MeV})\exp[-(r - R_t)/a] \tag{18}$$

where $a = 1{\cdot}2$ and $R_t = r_t(A_1^{1/3} + A_2^{1/3})$. In (16), the coupling process is mostly due to inelastic excitations and the form factor F_1 is estimated from the collective model expression

$$F_1 = \frac{1}{(4\pi)^{1/2}}(-\beta R)\frac{dV_n(r)}{dr}. \tag{19}$$

In simultaneous coupling, if one of the channels is transfer channel, the same form factor F_2 can be used for single particle transfer. However, in the present case we estimate F_1 from (19), so that all the non-elastic channels are due to inelastic excitations only. These schematic coupling schemes given in figures 7(a) and 7(b), represent two extreme situations. If either the target or the projectile have a few low-lying collective states, the collision process might excite these states first, before many sequential transfers take place. This picture will give rise to different coupling schemes which are shown schematically in figure 7(c). Even though, the sequential transfers are initiated from many low-lying inelastic states, we consider only one such state and accordingly the coupling matrix is given by

$$M_{\alpha\beta} = \begin{vmatrix} 0 & F_1 & 0 & 0 & 0 \\ F_1 & -Q & F_2 & 0 & 0 \\ 0 & F_2 & -Q & F_2 & 0 \\ 0 & 0 & F_2 & -Q & F_2 \\ 0 & 0 & 0 & F_2 & -Q \end{vmatrix}. \tag{20}$$

An exact solution can be obtained by using a more realistic coupled channel code as one used in ref. [10], where transfer process is treated more acurately. However, we adopt a simple method to study some of the general properties more qualitatively that arises under different coupling schemes and to compare these results with the barrier distribution that are extracted fitting experimental fusion cross sections. Therefore, instead of diagonalizing these matrices at each r, we diagonalize them at a fixed $r = R_0$. In other words, a constant form factor is assumed which is the representative value of the coupling strength at the unperturbed barrier position R_0.

The barrier distribution that results from different coupling schemes are obtained by calculating fusion cross-section as a function of energy and then numerically evaluating the quantity $d^2(E\sigma)/dE^2$. This is shown in figure 8. With the normal value of r_t and a, which are of the order of 1·2 (see ref. 18), the coupling strength is not enough to give rise to a broad distribution. In Rowley *et al* [10], a large spectroscopic value for transfer is used which is roughly twice its normal value. One way to increase the strength is to use a larger radius parameter r_t in (18) which can be justified from

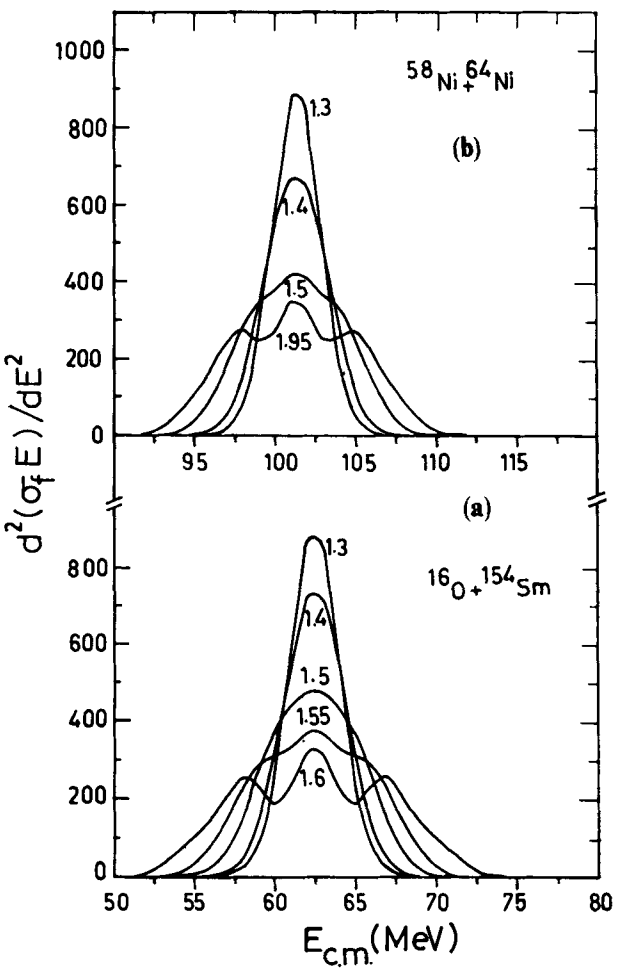

Figure 8(a, b). $d^2E(\sigma_f E)/dE^2$ versus $E_{c.m.}$ for $^{16}O + ^{154}Sm$ and $^{58}Ni + ^{64}Ni$ systems for sequential coupling scheme (figure 7(b)) with different values of r_t.

the fact that transfer can be initiated at a larger distance. Therefore, we treat r_t as a variable. Figure 8(a) shows the barrier distribution for $^{16}O + ^{154}Sm$ system and figure 8(b) for $^{58}Ni + ^{58}Ni$ system with different r_t values. It can be seen that the barrier distribution becomes broader with increasing value of r_t. There is a critical value of r_t at which the barrier distribution resembles with that of a flat barrier distribution. The similar trend is also seen for many other systems. It is interesting to note that r_t lies in the range of 1·4 to 1·6 fm for all the systems and is consistent with the r_0 values used in the analysis of the multinucleon transfer channels in the H.I. reactions. This suggests that the transfer process is initiated outside the Coulomb barrier and this value is practically same for all the systems. It can be mentioned here that these barrier distributions and the true barrier distributions that are discussed in § 2 are not same. For example, the barrier distribution for $^{16}O + ^{154}Sm$ is known to be asymmetric. The broad barrier distribution discussed here is only of academic interest as we want to study the effect of different coupling scheme on barrier distribution function irrespective of the system chosen.

In all these calculations, we had set Q value to zero. The results will be completely different with finite Q value. The barrier distribution for $Q = 0$, -3 and $+3$ MeV are shown in figure 9 for $^{16}O + ^{92}Zr$ system. Here again the choice of the system is arbitrary. The positive Q value makes barrier distribution more repulsive, while the negative value enhances the cross sections. This result is opposite to what happens in the case of simultaneous coupling. Moreover, the barrier distribution is no longer symmetric due to finite Q value effects. On the other hand, barrier distribution extracted from fitting the experimental fusion cross sections are rather flat for most of the systems, which suggests the sequential transfer with zero effective Q value as the most favoured one. As suggested in [19], this behaviour can be correlated to many repeated nucleon transfers between the orbitals of the two core nuclei such that the effective Q value is zero.

Next, we consider the effect of simultaneous coupling on barrier distribution $D(B)$ by diagonalizing the matrix given by (16). Figure 10(a) shows the plot of $d^2(\sigma_f E)/dE^2$ as a function of E_{cm} for $^{16}O + ^{92}Zr$ system for $n = 2, 3, 5$ with a typical β value of

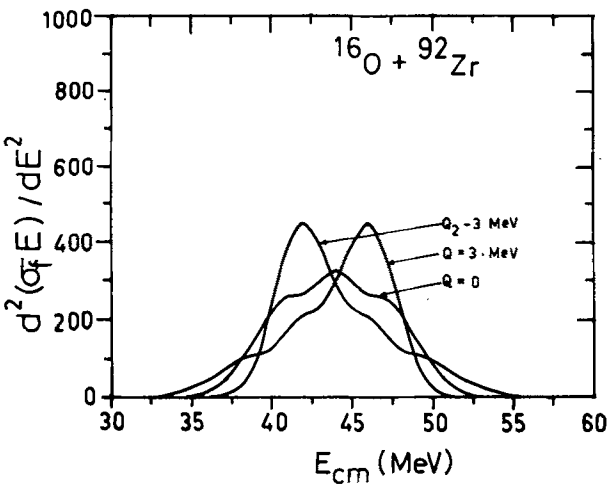

Figure 9. $d^2E(\sigma_f E)/dE^2$ versus $E_{c.m.}$ for $^{16}O + ^{92}Zr$ system for sequential coupling scheme (figure 7(b)) with $Q = -3$ MeV, O and $+3$ MeV.

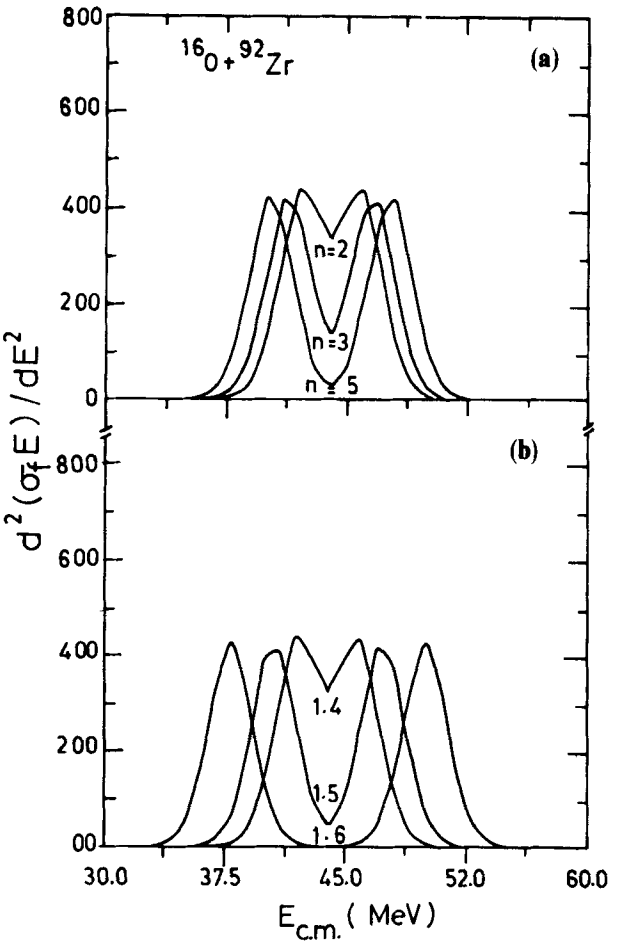

Figure 10(a). $d^2E(\sigma_f E)/dE^2$ versus $E_{c.m.}$ for $^{16}O + ^{92}Zr$ system for simultaneous coupling scheme (figure 7(a)) with $\beta_2 = 0{\cdot}25$ for different number of channels. **10(b).** Same as figure 10(a), but instead of F_1, the form factor F_2 is used with different r_t values for $n = 6$.

0·25. As expected [20], the barrier distribution shows double peaks and with more number of channels, the peaks are shifted further. Instead of number of channels, if the coupling strength is increased further, a similar behaviour in barrier distribution is seen. This is shown in figure 10(b) for $n = 5$ with form factor F_2 as a function of r_t. These calculations demonstrate that with the same coupling strength $r_t = 1{\cdot}6$ and $n = 6$, the sequential coupling gives a broad barrier distribution, while the simultaneous coupling results in a double hump distribution which can be understood either by increasing the number of channels or by increasing the coupling strength.

As seen from figure 2, although most of the system favours a flat barrier distribution, the barrier distribution for a few systems is of Gaussian type. This result cannot be understood on the basis of only simultaneous or sequential coupling studied so far. In order to obtain a Gaussian barrier distribution, we have to assume two different form factors F_1 and F_2 as given in (20). The basic assumption in this scheme is that before sequential transfer is initiated, the system gets coupled to low-lying inelastic states and thereafter sequential transfers follows. For simplicity, we have considered

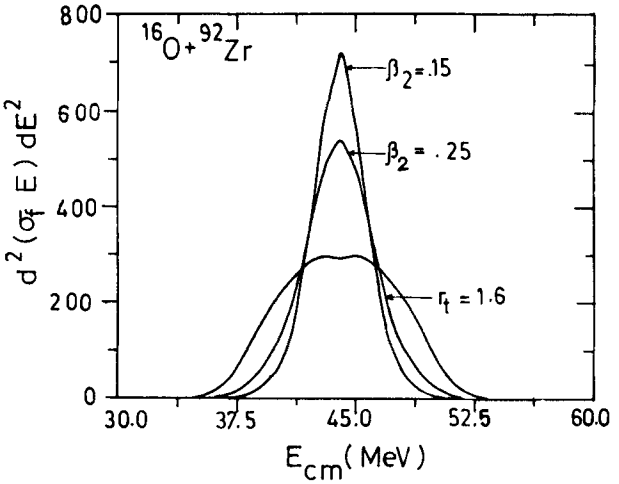

Figure 11. $d^2E(\sigma_f E)/dE^2$ versus $E_{c.m.}$ for $^{16}O + ^{92}Zr$ system. The sharp distribution corresponds to the coupling scheme given in figure 7(c) with $\beta_2 = 0{\cdot}25$ and $0{\cdot}15$. The broad distribution corresponds to the case of sequential coupling scheme with $r_t = 1{\cdot}6$.

only one inelastic state with form factor F_1. Figure 11 shows the plot of $d^2(\sigma_f E)/dE^2$ as a function of E_{cm} with two different β values of 0·25 and 0·15. The strength of F_2 is taken at $r_t = 1{\cdot}6$ fm. Replacement of F_1 with F_2 results in broad barrier distribution is also shown for comparison. Therefore, if we use F_1 different from F_2, the resultant distribution is of Gaussian type which is characteristic of many systems having low-lying collective states.

A study of low-lying levels of projectiles and targets for which the barrier distribution width is shown in figure 2, shows that Ge and Sm isotopes have more low-lying collective states in comparison to rest of the systems studied. Accordingly, the barrier distribution for the system where one of the partners is Ge or Sm, is of Gaussian type. It can also be seen, in comparison to $^{16}O + ^{150}Sm$, the barrier distribution is more sharp for $^{40}Ar + ^{144}Sm$, as Ar being a heavier projectile, the probability of inelastic excitation is higher in latter case than the former. It is also interesting to note that the barrier distribution of $^{58}Ni + ^{58}Ni$ and $^{64}Ni + ^{64}Ni$ are quite broad, whereas in $^{58}Ni + ^{64}Ni$, it is Gaussian. This can be understood on the basis of similar argument that this system is known to have a positive Q value $2n$ transfer channel. Therefore, this system couples simultaneously to the $2n$ channel with relatively small coupling strength F_2 (this form factor can be estimated from eq. (18) with $r_t = 1{\cdot}2$ fm.).

In summary, it is shown that, experimental fusion cross section for those systems which have less important collective degrees can be best explained by using a flat barrier distribution, while the systems having more collectiveness prefer a Gaussian barrier distribution. These various shapes of barrier distribution functions are generated by using a truncated Gaussian function where the width parameter δ and corresponding truncation limit t are fixed by χ^2 minimization. The optimal δt values for the systems which favour flat barrier distribution, increase monotonically with effective fissility ξ which can be correlated to the concept of neck formation or neutron flow which depends on the liquid drop properties of the colliding nucleus. Even though, a particular distribution function is favoured by a particular system, it is

seen that for those systems where the optimal t is small, many distribution functions can be used to get fusion cross section and average spin values which are indistinguishable from each other. However, these differences become prominent while comparing the second derivative $[d^2(\sigma_f E)/dE^2]$ obtained from different distribution functions. The observed different barrier distribution functions have been interpreted on the basis of a new model involving non-elastic processes in the framework of coupled channel formalism. It is known that the sequential coupling (due to multinucleon transfers) results in a broad barrier distributions which are quite similar to the flat barrier distributions often found necessary to fit the experimental fusion excitation functions. In the present work using a simple schematic model, it is also shown that the sequential coupling gives a very broad barrier distribution, while the simultaneous coupling results in a double hump distribution. As discussed before, although most of the system favours a flat barrier distribution, the barrier distribution for a few systems, having well developed collective states, are of Gaussian type. This result cannot be understood on the basis of either simultaneous or sequential coupling. Therefore, we have assumed a new coupling scheme wherein before sequential transfer is initiated, the system gets coupled to low-lying inelastic states and thereafter sequential transfers follows. This method results in Gaussian barrier distribution function.

Acknowledgements

We are very much thankful to Drs V S Ramamurthy, S S Kapoor, M A Nagarajan and S V S Sastry for illuminating discussions on several aspects of this study.

References

[1] M Beckerman, *Rep. Prog. Phys.* **51**, 1047 (1988)
[2] C H Dasso, S Landowne and A Winther, *Nucl. Phys.* **A405**, 381 (1983)
C H Dasso, S Landowne and A Winther, *Nucl. Phys.* **A407**, 221 (1983)
[3] I J Thompson, M A Nagarajan, J S Lilley and B R Fulton, *Phys. Lett.* **B157**, 250 (1985)
[4] S C Pieper, M J Rhoades-Brown and S Landowne, *Phys. Lett.* **B162**, 43 (1985)
[5] C E Aguiar, V C Barbosa, L F Canto and R Donangelo, *Nucl. Phys.* **A472**, 571 (1987)
A Iwamoto and K Haroda, *Z. Phys.* **A326**, 201 (1987)
[6] V S Ramamurthy, A K Mohanty, S K Kataria and G Rangarajan *Phys. Rev.* **C41**, 2702 (1990)
[7] H Esbensen, *Nucl. Phys.* **A352**, 147 (1981)
[8] P H Stelson, *Phys. Lett.* **B205**, 190 (1988)
[9] P H Stelson, H J Kim, M Beckerman, D Shapira and R L Robinson, *Phys. Rev.* **C41** 1584 (1990)
[10] N Rowley, *Nucl. Phys.* **A538**, 205c (1992)
N Rowley, I J Thompson and M A Nagarajan, *Phys. Lett.* **B282**, 27 (1992)
[11] J X Wei *et al*, *Phys. Rev. Lett.* **67**, 3368 (1991)
[12] C Y Wong, *Phys. Rev. Lett.* **31**, 766 (1973)
[13] W Reisdorf *et al*, *Nucl. Phys.* **A438**, 212 (1985)
[14] C E Aguair, A N Aleixo, V C Barbosa, L F Canto and R Donengelo, *Nucl. Phys.* **A500**, 195 (1989)
[15] H J Krappe, K Mohring, M C Nemes and H Rossner, *Z. Phys.* **A214**, 23 (1983)
[16] N Rowley *et al*, *Phys. Lett.* **B254**, 25 (1991)
[17] C H Dasso and S Landowne, *Phys. Lett.* **B183** 141 (1987)
[18] R A Broglia, G Pollarolo and A Winther, *Nucl. Phys.* **A406**, 369 (1983)

[19] B Imanishi and W Von-Oertzen, *Phys. Rep.* **155**, 29 (1987)
[20] A T Krupa, P Romain, M A Nagarajan and N Rowley, Preprint DL/NUC/P324T, Daresbury 1992
[21] R G Stokstad *et al*, *Phys. Rev.* **C21**, 2427 (1980)
[22] A H Wuosmaa *et al*, *Phys. Lett.* **B263**, 23 (1991)
[23] M Beckerman *et al*, *Phys. Rev.* **C23**, 1581 (1981)
M Beckerman *et al*, *Phys. Rev.* **C25**, 837 (1982)
[24] M DasGupta *et al*, *Nucl. Phys.* **A539**, 351 (1992)